THE ASTROPHYSICAL JOURNAL, 449:18–27, 1995 August 10

GRAVITATIONAL LENSING IN CLUSTERS OF GALAXIES: NEW CLUES REGARDING THE DYNAMICS OF INTRACLUSTER GAS

JORDI MIRALDA-ESCUDÉ[1,2] AND ARIF BABUL[3,4]
Received 1994 March 18; accepted 1995 February 15

ABSTRACT

Long arcs in clusters of galaxies, produced by gravitational lensing, can be used to estimate the mass interior to the arcs and therefore constrain the cluster mass distribution. The radial density distribution of the intracluster gas can be extracted from the X-ray surface brightness observations. If the gas temperature is also known, it is then possible to probe the dynamical state of the gas and in particular, to test the hypothesis that the intracluster gas is in hydrostatic equilibrium within the gravitational potential of the cluster as a result of thermal pressure support.

We analyze three clusters that exhibit large arcs, whose X-ray surface brightness profiles have been observed, and whose gas temperatures have been determined. In two of the clusters, A2218 and A1689, the central mass implied by lensing is a factor of 2–2.5 too large for the gas at the observed temperature to be in hydrostatic equilibrium solely due to thermal pressure support. In other words, if we accept the mass estimate derived from the lensing analysis and demand that the X-ray surface brightness profile be consistent with the observations, the temperature of the gas has to be a factor of 2–2.5 larger than the observed value. The results for the third cluster, A2163 (the most luminous and the hottest cluster known), are more ambiguous.

The discrepancy between the X-ray and the lensing mass estimates arise because the presence of arcs implies a highly concentrated cluster mass distribution whereas the observed X-ray profiles imply a more extended mass distribution. The large X-ray core radii are not the result of the limited resolution of the X-ray detectors. We consider various possibilities that could account for the discrepancy.

Subject headings: gravitational lensing — intergalactic medium

1. INTRODUCTION

It has long been recognized that mass concentrations can gravitationally lens light rays from background sources and that such images offer the possibility of probing the matter distribution in the lensing bodies (e.g., Einstein 1936; Zwicky 1937). Soon after the discovery of the first gravitational lenses (Walsh, Carswell, & Weymann 1979), several authors considered the possibility that clusters of galaxies could act as gravitational lenses, noting that if the cluster mass distribution is sufficiently concentrated toward the center, they would be able to produce images with splitting angles as large as 60″ (Turner, Ostriker, & Gott 1984; Narayan, Blandford, & Nityananda 1984). The discovery of arcs in clusters of galaxies, and their subsequent confirmation as gravitationally lensed images of background galaxies (Soucail et al. 1987; Lynds & Petrosian 1989), provided the first hints that the mass distribution in these clusters is indeed highly concentrated (e.g., Grossman & Narayan 1988). In fact, in most lensing clusters, the mass needs to be more concentrated than the gas distribution that is inferred from the X-ray profile (Grossman & Narayan 1989; Miralda-Escudé 1993; Wu & Hammer 1993), which typically have core radii of $\sim 300\ h_{50}^{-1}$ kpc (e.g., Jones & Forman 1984; Edge & Stewart 1991).

By using X-ray and lensing observations in conjunction, we can learn much more on the relative distributions of the gas and the mass in clusters, and on the physical state of the gas (Kellogg et al. 1990). In this paper, we use the observed arcs to estimate the total mass within a central region in the clusters and, in combination with the X-ray temperature and surface brightness measurements, test if this is consistent with the generally accepted hypothesis that the hot gas in clusters is in hydrostatic equilibrium as a result of thermal pressure support. Specifically, we consider three clusters: A2218, A1689, and A2163. Highly distorted arcs have been observed in all three. Furthermore, the X-ray properties, including the X-ray surface brightness profile and the temperature of the X-ray–emitting intracluster gas, of all three clusters have been measured and well studied. The X-ray and the optical properties of the three clusters are summarized in Table 1. We use the observed arcs to estimate the total projected mass within the radius of the arcs, and therefore constrain the cluster potential. Since the temperature of the gas is also known, we then explore whether it is possible for the intracluster gas to exist in thermal pressure-supported hydrostatic equilibrium in the constrained cluster potential, and produce X-ray surface brightness profiles consistent with those observed. Throughout this paper, we assume an Einstein–de Sitter model for the universe ($\Omega = 1$) and adopt a Hubble constant of $H_0 = 50$ km s^{-1} Mpc^{-1}. Our method will be described in § 2, and the results are presented in § 3. Possible interpretations of the results are discussed in § 4. Finally, in § 5 we summarize our findings and suggest directions for future theoretical and observational work.

[1] Institute for Advanced Study, Princeton, NJ 08540; jordi@guinness.ias.edu.

[2] Institute of Astronomy, Madingley Road, Cambridge CB3 0HA, England, UK.

[3] Canadian Institute for Theoretical Astrophysics, 60 St. George Street, Toronto, Ontario M5S 1A1, Canada.

[4] Department of Physics, New York University, 4 Washington Place, New York, NY 10003; babul@alMuhit.physics.nyu.edu.

2. METHOD OF ANALYSIS

In gravitational lensing, highly elongated arcs lie very close to the "critical line" of a cluster. In a spherical potential, the critical line traces a circle. Strictly speaking, a highly elongated

TABLE 1

CLUSTER PROPERTIES

Cluster	z	L_x(2–10 keV) ($\times 10^{45}$ ergs s^{-1})	kT_x (keV)	R	σ_r (km s^{-1})
A1689.....	0.17	2.8	8.0	4	1800
A2163.....	0.20	7.0	13.9	2	...
A2218.....	0.17	1.0	6.7	4	1370

arc in a spherically symmetric potential should always be accompanied by a counterarc of approximately the same length on the opposite side of the lens; however, the slightest deviation from spherical symmetry will cause the counterarc to shrink in size or even disappear altogether. Therefore, we will not be concerned about the counterarc and assume that the observed arc is coincident with the critical line.

The mean projected surface mass density within the critical circle of angular radius b in a spherical potential is

$$\bar{\Sigma}(b) = \Sigma_{\rm crit} = \frac{c^2}{4\pi G}\left(\frac{D_s}{D_l D_{ls}}\right), \quad (1)$$

where D_l, D_s, and D_{ls} are the angular diameter distances to the lens, to the source, and from the lens to the source, respectively (e.g., Blandford & Kochanek 1987). The projected mass within the critical circle (i.e., the mass contained within a cylinder of angular radius b passing through the center of the cluster) is

$$M_p(b) = \Sigma_{\rm crit}\,\pi b^2 D_l^2\ . \quad (2)$$

The above relationship, between the radius of an arc (critical line) and the projected mass contained within, is relatively insensitive to small deviations from sphericity. We shall use this relation as a basic constraint obtained from lensing, corrected by an appropriate factor to take into account the deviations from spherical symmetry in the models for the mass distributions that are designed to reproduce the observed arcs (see § 3).

We consider two different parameterized density profiles for the mass distribution in the clusters:

$$\rho(r) = \frac{\rho_0}{[1 + (r/r_c)^2]^{\gamma/2}} \times \left(1 + F_{cD}\,\frac{r_c^2}{r^2 + r_{cD}^2}\right), \quad (3)$$

$$\rho(r) = \frac{\rho_0}{(r/r_c)^{\alpha}(1 + r/r_c)^{\gamma-\alpha}}\ . \quad (4)$$

In both cases, the overall normalization, denoted by ρ_0, is fixed by equation (2) once all the other free parameters are defined. In the first profile (eq. [3]), the density falls off as $r^{-\gamma}$ at large radii, flattens at intermediate radii, and may steepen again at some smaller radii, simulating the influence of a cD galaxy whose importance is quantified by the parameter $F_{\rm cD}$. In total, there are three free parameters: the core radius r_c, the slope at large radius γ, and $F_{\rm cD}$. We fix the value of the galaxy core radius at $r_{\rm cD} = 0''.1$; small deviations about this value have no effect on the observable properties (the parameter $r_{\rm cD}$ is introduced only for ease in the numerical calculations). In the second profile, the density drops as $r^{-\alpha}$ for $r \ll r_c$ and as $r^{-\gamma}$ for $r \gg r_c$, where r_c is the core radius. This mass profile also has three free parameters: r_c, γ, and α.

We assume that the gas in the cluster potential defined by the above mass distributions is in hydrostatic equilibrium and obeys the polytropic equation of state: $p \propto \rho_g^{\gamma_T}$. The radial distribution of the gas is, therefore, prescribed by

$$\frac{d\log \rho_g}{d\log r} = -\frac{GM(r)\mu}{\gamma_T kT(r) r}\ , \quad (5)$$

where μ is the mean mass per particle in the gas (we adopt a value of $\mu = 0.6 m_p$), and $M(r)$ is the total mass contained within a sphere of radius r. In most of our models, we will assume that the gas is isothermal (i.e., $\gamma_T = 1$).

Once the gas density is determined, we compute the model X-ray surface brightness by approximating the thermal bremsstrahlung emissivity of the intracluster gas, in a fixed energy band, as $\epsilon \propto \rho_g^2 T^{-0.3}$ and by integrating along the line of sight (the dependence on temperature depends on the sensitivity of the X-ray detector at different photon energies; our adopted dependence is a good approximation for instruments with maximum sensitivities at energies somewhat lower than the redshifted cluster temperature, which is often the case). In order to compare the computed X-ray surface brightness with the observations, we convolve the computed surface brightness with the detector point spread function and integrate the flux in radial bins. We then vary the free parameters in the assumed mass profile until we achieve the best possible fit to the observations that minimizes χ^2. We note that this procedure is completely equivalent to the way in which X-ray profiles have been analyzed in the literature but with the crucial difference that we enforce the mass constraint imposed by the lensing analysis (eq. [2]).

3. RESULTS

3.1. *A2218: the Lensing Constraint*

We begin with an analysis of A2218; the preliminary results of our work for this cluster were reported in Miralda-Escudé & Babul (1994). A2218 is an Abell richness class 4 cluster at a redshift of $z_l = 0.175$ (LeBorgne, Pelló, & Sanahuja 1992), with an X-ray luminosity in the 2–10 keV band of $L_x = 1 \times 10^{45}$ ergs s^{-1} (David et al. 1993). The radial velocity dispersion of the cluster galaxies is 1370 km s^{-1} (LeBorgne et al. 1992) and the cluster's X-ray temperature has been determined by McHardy et al. (1990) to be 6.7 keV or 7.8×10^7 K. For the present purposes, we will adopt a value of $T_x = 8 \times 10^7$ K. The optical image of A2218 (see Pelló et al. 1988, 1992) reveals the existence of several arcs around a central cD galaxy, as well as two arcs close to another bright galaxy, located 67″ away from the cD galaxy, that seems to define a secondary mass clump. The location and the morphology of the latter two arcs, the relative luminosity of the two bright galaxies, and the concentration of other galaxies around them, suggest that the second mass concentration is much smaller than that around the cD galaxy. Furthermore, the X-ray peak in the *ROSAT* PSPC image of A2218 (Stewart et al. 1994) appears to be coincident with the location of the cD galaxy. Consequently, we designate the cD galaxy as the center of the cluster and focus on the associated large arcs.

In Figure 1, we show an example of a model reproducing the observed arcs. The images of two background sources assumed to be circular are plotted as solid curves. The crosses indicate the positions of the two bright galaxies (plus a third one close to the secondary galaxy), and the dotted lines are critical lines at two different observed redshifts of the arcs: 0.702 and 1.034. Analysis of arcs in other clusters has shown that, in general, the cluster mass distribution can be modeled as being composed of massive halos associated with the brightest galaxies, having

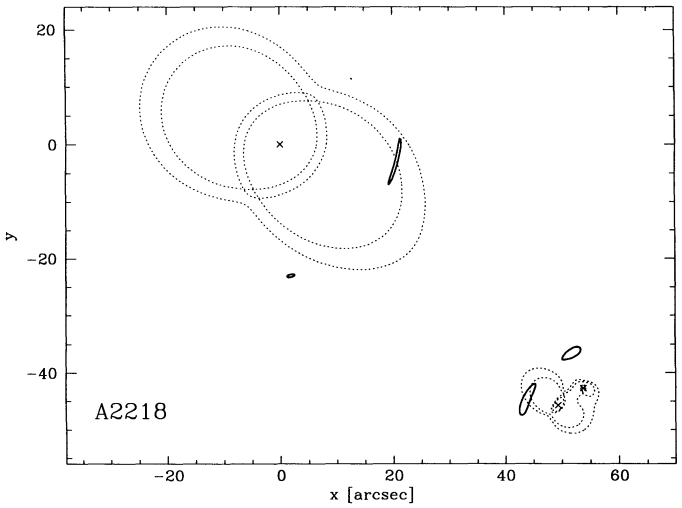

FIG. 1.—An example of a gravitational lensing model that reproduces some of the observed arcs in the cluster A2218, from two circular sources in the background. The cross at the coordinates origin indicates the position of the central cD galaxy, and the other two crosses are the centers of two galaxies in a secondary clump of mass (no. 244 and no. 259 in Pelló et al. 1992). One source, at $z = 0.702$, produces a fold arc and another image around the main clump, shown as solid curves (the isophote shown is for an angular radius of the source of 0.″15). Another source at $z = 1.034$ produces the arc close to the secondary clump (the arc is broken into two images for this isophote, corresponding to a source radius of 0.″5, but for a slightly larger radius they would be joined together). The dotted lines are critical lines at the two source redshifts. The density profiles of the lenses are described by model 1 (eq. [3]) but with $F_{cD} = 0$. The remaining parameter are as follows: the clump centered on the central galaxy has $\sigma \equiv (2\pi G\rho_0 r_c^2)^{1/2} = 1200$ km s^{-1}, $r_c/D_l = 10''$, with an ellipticity for the surface density $\epsilon = 0.3$, and position angle of the major axis $\phi = -30°$, similar to the ellipticity and position angle of the cD stellar halo (we use the quadrupole approximation to calculate the potential). At $x = 49.''3$, $y = -45.''7$, two superposed clumps model galaxy no. 244 and an assumed extended dark matter halo, with the parameters $\sigma = 350$ km s^{-1}, $r_c/D_l = 2''$, and $\sigma = 230$ km s^{-1}, $r_c/D_l = 0.''2$, both with $\epsilon = 0.15$ and $\phi = -30°$. At $x = 53.''7$, $y = -42.''7$, another clump modeling a smaller galaxy (no. 259) has $\sigma = 200$ km s^{-1}, $r_c/D_l = 0.''2$, $\epsilon = 0.1$, and $\phi = 10°$.

similar ellipticities as the luminous envelopes of these galaxies (Mellier, Fort, & Kneib 1993; Kneib et al. 1993). This is not surprising, since the stellar halos of the bright galaxies centered on the arcs can often be seen to radii larger than that of the arcs. Following this prescription, our model assumes the presence of elliptical halos with the profile of our model 1 (eq. [3]), but with $F_{cD} = 0$, centered on the two bright galaxies and also on a smaller galaxy in the secondary clump. We use the quadrupole approximation for elliptical potentials, using the same formalism as in Miralda-Escudé (1993). The model parameters are given in the figure caption. More detailed modeling of the lensing in this cluster is presented in Kneib et al. (1994).

The object no. 359 in Pelló et al. (1992) has a measured redshift of 0.702 (see also Petrosian & Lynds 1992) and is 20.″8 from the central galaxy. There is another object, no. 328 in Le Borgne et al. (1992), which is very likely another image of the source producing the arc no. 359. The model we show can easily reproduce the position and ellipticity of this image. If that is correct, then the arc no. 359 should be a double image on a fold catastrophe, with possibly a part of the arc being eclipsed by the cluster galaxy no. 373 (see Fig. 4 in Pelló et al. 1992). The critical line should, therefore, intersect this arc, as is seen in the model of Figure 1. In subsequent discussion, we adopt $b = 20.''8$ as the critical radius around the cD galaxy in A2218, for a source at $z_s = 0.702$. Another arc, no. 289, is also reproduced by the model.

In the mass model described above, the average surface density in a circle centered on the cD galaxy and whose radius corresponds to the distance to the arc no. 359 is slightly smaller (87%, of which 84% is due to the main clump around the cD galaxy and 3% is due to the secondary clump) than the critical value implied by equation (1). This difference in value of the surface density is quite insensitive to the variations in the details of the mass models, as long as the mass models can successfully reproduce the positions and the elongations of the arcs, and arises because the mass model of Figure 1 is aspherical while equation (1) is correct only for spherical potentials. In the mass model, the distance to the critical line at the location of the arc is larger than in the spherical case, an effect that can be attributed to two causes: First, the halo around the cD galaxy is elliptical and the ellipticity moves the critical line outward along the major axis, and second, there exists a secondary mass concentration that also draws the critical line toward it.

To fit the X-ray surface brightness profile for A2218, we adopt the standard assumption that the intracluster gas exists in hydrostatic equilibrium within the cluster potential. We consider only spherical models for the cluster mass distribution and impose the basic lensing constraint by requiring that the mass distribution have a critical radius of $b = 20.''8$. As discussed above, however, deviations from spherical symmetry (e.g., two mass clumps) are necessary to reproduce the observed arc images (see Fig. 1). We account for the major difference between the spherical and aspherical lensing models by allowing for the possibility that value of the critical surface density derived from equation (1) may be a factor of ~ 1.2 too high. With respect to the gas distribution, our models are based on the assumptions that (1) the presence of the second mass clump does not affect the equilibrium state of the gas in any significant way and (2), the ellipticity of the mass distribution does not greatly influence the profile of the gas distribution. Under these assumptions the X-ray profiles derived from the spherical and aspherical models will not differ in any significant way.

The second assumption, that the ellipticity of the mass distribution should not greatly influence the gas profile, is reasonable. In fact, gas distribution will not even be as elliptical as the mass distribution. A gas distribution in hydrostatic equilibrium traces the equipotential surfaces, and these surfaces are rounder than the underlying mass distribution. The presence of a second mass clump, however, calls into question the assumption that the gas is in hydrostatic equilibrium. The latter assumption can be correct only if the secondary clump is sufficiently small and that the gravity of the clump, as well as the ram pressure of the gas associated with it, only weakly disturbs the gas associated with the main cluster body. In any case, we see that the presence of substructure puts in doubt the validity of equation (5). This will be discussed further in § 4.

3.2. *A2218: Results of X-Ray Fits for Isothermal Models*

In Figure 2*a*, the observed X-ray surface profile of A2218 derived from the *ROSAT* PSPC image is shown by the error bars (Stewart et al. 1994). We first obtain a fit with our model 1 (eq. [3]), by χ^2 minimization, subject to the lensing condition of equation (1). We restrict the parameter space to be searched by imposing the following constraints on the possible range of the free parameters: $\gamma > 1.5$, and $r_c < 1$ Mpc. Models with param-

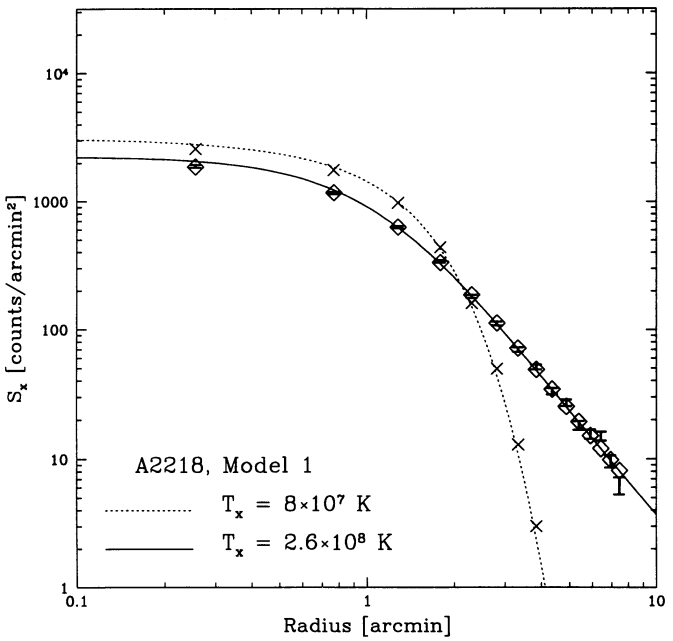

FIG. 2a

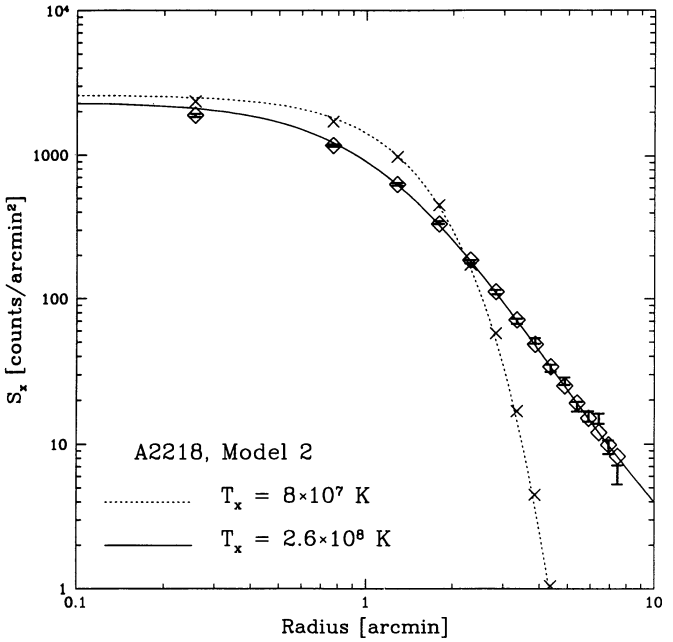

FIG. 2b

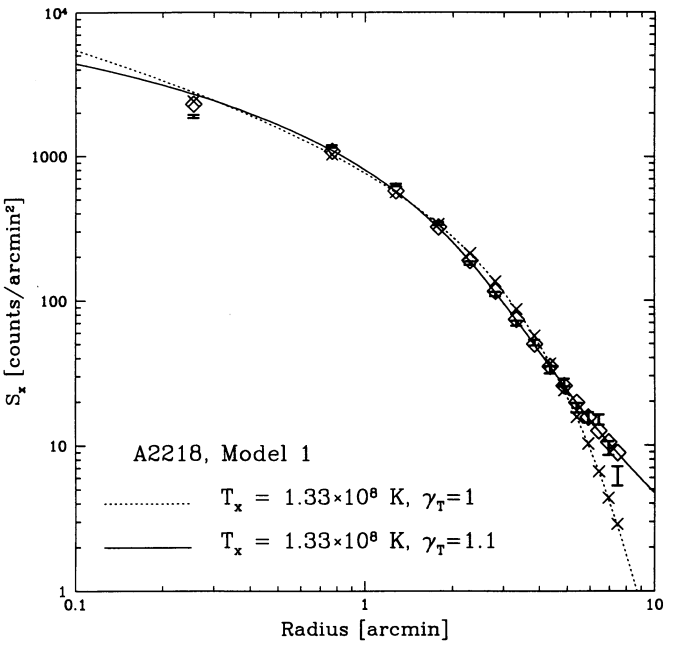

FIG. 2c

FIG. 2.—Model fits to the X-ray surface brightness profile derived from the *ROSAT* PSPC image of A2218. The surface brightness is in counts cm^{-2}. The error bars are observations, the solid and dotted lines are the model results, and the diamonds (*crosses*) result from convolving the solid (*dotted*) lines with the detector point spread function and integrating into the same bins as the observations. In Fig. 2*a*, the dotted line shows the best fit (minimum χ^2) surface brightness associated with model 1 mass distribution and isothermal gas with $T_x = 8 \times 10^7$ K. The mass distribution is normalized using the lensing constraint of eq. (1). In comparison to the observations, the model fit is unacceptable, with $\chi^2 = 4194$. The solid line shows the best-fit curve when the gas temperature is raised by a factor 3.25 (or equivalently, the surface density within the critical radius is reduced by the same factor); the fit is acceptable with $\chi^2 = 16.0$. Fig. 2*b* is the same but for model 2 of the mass distribution, and the same results are found. In Fig. 2*c* we compare the fits to the data due to model 1 mass distribution coupled with isothermal and polytropic gas (with $\gamma_T = 1.1$, where $T \propto \rho_g^{\gamma_T - 1}$) distributions. The isothermal model fit is characterized by $\chi^2 = 429$, and the polytropic one by $\chi^2 = 138$. A rising temperature to the center can therefore alleviate the problem, although it may not be possible to solve it entirely without engendering large temperature gradients that ought to be observable.

eters beyond these ranges imply a very high velocity dispersion for the cluster galaxies at large radius (the physical reason why such a constraint needs to be imposed will be made clear below). The dotted line in Figure 2*a* shows the X-ray profile for the best fit obtained by pegging the gas temperature to its observed value, $T_x = 8 \times 10^7$ K. The crosses are the predicted fluxes in the same radial bins as the observed fluxes, after convolution with the point spread function, which we take to be Gaussian with FWHM = 31″. The parameters of the model (see eq. [3]) are $r_c = 1$ Mpc, $\gamma = 1.5$, $F_{cD} = 0.005$. This is at the boundary of the region we allow, and it implies that the preferred model has a very extended mass distribution, with a small peak in the center. It is clear from the figure that the fit is totally unacceptable. The χ^2 is 4194, while the expected value is 11. This model is, therefore, ruled out.

The solid line in Figure 2*a* is the best-fit X-ray profile, for the mass profile of model 1, when the gas temperature is $T_x = 2.6 \times 10^8$ K, a factor of 3.25 higher than the observed value. The diamonds show the predicted fluxes in the observed bins, after convolution. The parameters associated with this fit are $r_c = 0.24$ Mpc, $F_{cD} = 0.018$, and $\gamma = 2.49$, and the χ^2 for the fit is 16.0, an acceptable value. This model has the minimum χ^2 when the temperature is left as a free parameter. If the temperature is fixed at 2.5 times the observed value, the resulting best fit (with respect to the three parameters of model 1) surface brightness profile has $\chi^2 = 40.6$ and if the temperature is only increased by a factor of 2, then the best-fit profile has $\chi^2 = 200$. Raising the temperature of the gas by a factor of 3.25 is equivalent to reducing the required surface density within the critical radius in equation (1) by the same factor (see eq. [5]). This reduction, however, is much greater than the factor of ~ 1.2 that can be attributed to deviation of the cluster mass distribution from spherical symmetry.

In constructing our spherical models, we have imposed only equation (1) as a constraint from the lensing observations. This, however, is the basic lensing constraint, and not the only constraint that must be satisfied. For example, the best-fit mass model in Figure 2 (*solid line*) has a very large core radius (approximately 3 times the radius of the arc), implying an almost constant surface density within the arc. Such large core radii are ruled out by the widths and curvatures of the observed arcs (Grossman & Narayan 1988; Hammer 1991; Miralda-Escudé 1993). In order to satisfy the additional constraints imposed by the morphology of the arcs, we can modify the current best-fit spherical mass model by either increasing F_{cD} or by requiring the core radius for the mass distribution to be small. Both modifications eliminate the flattened mass profile interior to the arcs, and can give rise only to greater discrepancies between the predicted and the observed X-ray surface brightness profile than found in our analysis.

In Figure 2*b* analogous models are shown for model 2 (eq. [4]). The dotted line and solid lines correspond to models with gas temperature $T_x = 8 \times 10^7$ K and $T_x = 2.6 \times 10^8$ K, respectively. The parameters for the best-fit $T_x = 8 \times 10^7$ K model are: $r_c = 1$ Mpc, $\alpha = 0$, and $\gamma = 1.5$. This model presents a poor fit to the observations ($\chi^2 = 3818$). When the gas temperature is a factor of 3.25 higher, the best-fit model has $r_c = 0.37$ Mpc, $\alpha = 0$, and $\gamma = 3.43$, with $\chi^2 = 16.9$. As in the case of model 1, the best-fit model for this value of the temperature yields the minimum χ^2. When the temperature is higher than observed only by a factor of 2.5 (2), the resulting best-fit models have $\chi^2 = 62$ (205). Again, the effective pressure of the intracluster gas must be a factor of ~ 3 greater than the thermal pressure of the gas estimated using observed X-ray temperature in order to simultaneously fit the observed X-ray surface brightness data and the basic gravitational lensing constraint. Alternatively, good fits to the observed X-ray surface brightness profile can be achieved by fixing the gas temperature at its observed value but reducing the projected mass internal to the critical radius by a factor of ~ 3 below the critical value. Deviations from spherical symmetry can account for only a reduction of a factor of 1.15–1.2.

The nature of the above discrepancy can be more easily understood if we assume that the cluster mass distribution is described by a singular isothermal sphere, $\rho \propto r^{-2}$, and has a velocity dispersion σ. The critical radius of such a cluster is (see Blandford & Kochanek 1987)

$$b = \frac{4\pi\sigma^2}{c^2} \frac{D_{ls}}{D_s} . \tag{6}$$

If the mass is assumed to have the same velocity dispersion as the gas, then $\sigma = (kT/\mu)^{1/2} = 1050$ km s^{-1}, and the critical radius for a source at redshift $z_s = 0.7$ is $b = 21''$, the same radius as that implied by the arcs. In this model, however, the gas profile is the same as that for the mass and the resulting X-ray profile diverges at small radius as r^{-3}. In order to flatten the X-ray profile within the central 1′ as observed, a core of approximately the same size must be introduced in the mass distribution. However, if we require that the projected mass within 20″ be unchanged (the lensing constraint) and do not alter the mass profile at large radii, then the velocity dispersion of the resulting cluster will be higher than that computed above. Furthermore, since the temperature of the gas is fixed, the gas density profile will need to be steeper and more peaked in order to satisfy the conditions for hydrostatic equilibrium. Alternatively, the lensing constraint can be satisfied by adjusting the cluster mass profile beyond the largest radius at which the X-ray flux is detected by making it more extended. The additional mass will affect neither the cluster velocity dispersion nor the observed X-ray profile; on the other hand, it will contribute to the projected surface density within the critical radius. Such a model would be consistent with all observations. However, the model is completely unrealistic. Even if the cluster had a profile with a constant density beyond the radius where X-rays are detected, the density profile would have to stretch out much further than the turnaround radius in order to increase significantly the surface density within the arcs. The presence of these physically unrealistic solutions to the discrepancy we find explains why it is necessary to impose an upper limit on the core radius r_c and a lower limit to γ in our models.

3.3. *A2218: Models with Increasing Temperature to the Center*

Thus far, we have considered only cases where the intracluster gas is isothermal. The solid line in Figure 2*c* shows the X-ray surface brightness profile for intracluster gas obeying the polytropic equation of state (i.e., $p \propto \rho_g^{\gamma_T}$), with $\gamma_T = 1.1$, in the best-fit model where the emission-weighted temperature is fixed to $T_x = 1.33 \times 10^8$ K, a factor of 1.66 higher than the observed value. T_x is defined as the average temperature of the gas, weighting every spherical shell by the total X-ray flux it emits, assuming that the flux emitted per unit volume is proportional to $\rho_g^2 T^{-0.3}$, as described in the end of § 2. The parameters for this model are $r_c = 1$ Mpc, $F_{cD} = 0.06$, and $\gamma = 6.65$, with $\chi^2 = 138$. The dotted line shows the best fit of the isothermal model with the same temperature, with parameters $r_c = 0.94$ Mpc, $F_{cD} = 0.163$, $\gamma = 1.5$, and $\chi^2 = 429$. The fit to the observed X-ray surface brightness profile is better when $\gamma_T = 1.1$. When the emission-weighted temperature is fixed at 1.6×10^8 K, then $\chi^2 = 36$ for $\gamma_T = 1.1$, practically acceptable. The reason is that in the polytropic model the temperature rises toward the center, and it is higher within the radius of the arc compared to the average temperature (in the model in Fig. 2*c*, the average temperature within the arc is 1.6×10^8 K). This causes the gas to be more extended for the same observed temperature. However, the variation of the temperature cannot solve the entire problem, since the temperature still needs to be fixed to a higher value than observed. Higher values of γ_T would allow us to lower the required temperature even more, but the temperature gradients they imply would probably have been observed. In any case, the problem we find will certainly be alleviated if cluster temperatures are found to increase to the center, while it will be exacerbated if they are found to decrease.

3.4. *A1689: the Lensing Constraint*

Next, we analyze the cluster A1689. A1689 is also an Abell richness class 4 cluster at a redshift of $z_l = 0.17$, with an X-ray luminosity in the 2–10 keV band of $L_x = 2.8 \times 10^{45}$ ergs s^{-1} (David et al. 1993). The radial velocity dispersion of the cluster galaxies is approximately 1800 km s^{-1} (Gudehus 1989), and the X-ray temperature of the intracluster gas is $kT_x = (7.6 \pm 0.5)$ keV (Yamashita 1994a, b). We shall adopt $T_x = 9.5 \times 10^7$ K, close to the upper limit. The galaxy distribution suggests two distinct galaxy aggregates. The largest concentration is very dense and it contains the merged images of various bright galaxies, and a smaller concentration is located approximately 1′ away in the northwest direction.

The larger of the two clumps is centered on galaxy no. 82 (we use the labels assigned by Gudehus & Hegyi 1991 in order to identify the galaxies in the cluster). We designate this galaxy as the center of the cluster. The location of the X-ray peak in the *Einstein* IPC image of A1689 is consistent with the location of galaxy no. 82; a *ROSAT* image of the cluster should be able to establish this better.

Deep optical images of the cluster (Tyson, Valdes, & Wenk 1990) reveal a few very long arcs of very low surface brightness among a large number of weakly but coherently distorted images of faint, blue, presumably background, galaxies. The distortion of these images gives strong evidence for gravitational lensing by the cluster, as emphasized by Tyson et al. The long arcs are clearly visible when the scaled *R*-band image of the cluster is subtracted from the *B*-band image (see Fig. 2 of Tyson et al. 1990). Three of the long arcs are located close to the cluster center and two are located near galaxies 145 and 151 in the secondary clump. Although none of the arcs has a measured redshift, their length, tangential elongation, and curvature are very strongly suggestive of the gravitational lensing interpretation.

The two arcs located in the secondary galaxy clump are probably not good indicators of the critical radius of the cluster, since their elongation should be mostly due to the secondary clump. Of the arcs near the cluster center, an approximately 10″ long arc lies 8″ northwest of galaxy 62 and at a distance of 47″ from the cluster center. Another arc, a brighter but shorter one, is located close to galaxy 25 at a distance of 43″ from the center. Finally, the longest arc in A1689 (20″ long) occurs near galaxy 167. It is curved around the center of the cluster, at a radius of 46″. We shall use this arc in order to estimate the critical radius. Most likely, it is a fold arc intersecting the critical line. We adopt a value of $b = 45''$ for the critical radius. As for the redshift of the background source, we can place an upper limit of $z_s = 4$ since the arc does not appear to have suffered a drop in the *B*-band flux that would occur when the Lyman break redshifts past 4500 Å. In fact, we adopt a source redshift of $z_s = 3$. The critical surface density is almost the same for a source located in the redshift range $3 \leq z_s \leq 4$, and a source redshift higher than $z_s = 3$ appears to be implausible because all of the arcs with measured redshifts lie at $z < 3$. If anything, the source is probably at a lower redshift, in which case our estimate of the projected mass required for lensing will be an underestimate. We note that although the shorter, brighter arc is only 43″ from the center, we believe that the smaller radius is due to the source being at lower redshift than the source for the longest arc, a likely explanation given the higher surface brightness of the shorter arc.

In Figure 3, we give a model which reproduces the longest arc around the main clump, and one of the arcs in the secondary clump. The model assumes two spherical clumps corresponding to the two groups of galaxies in the cluster center, with positions indicated by the two crosses. The coordinates in Figure 3 are centered on the main clump. The dotted lines denote the critical lines. One source produces one of the arcs close to the secondary clump, with no additional images; a second source, assumed to be at the same redshift, yields the longest arc, with three additional images: two arclets, and a demagnified image close to the center. The arclets might be hard to detect, due to their faintness and the crowded nature of the field. Their position is highly sensitive to the ratio of masses of the two clumps, and their quadrupole moments (here, we have assumed them to be spherical). We do not attempt to build an accurate model for reproducing all the arcs perfectly; our aim is only to determine the effect of deviations from spherical symmetry on the average surface density within a circle centered on the main clump and whose radius equals the distance to the long arc. According to this aspherical mass model, the contribution to the average surface density in the circle due to the main clump is 94% of the critical value (eq. [1]). Adding in the contribution from the second clump, the average surface density rises to 104%. The total projected mass within the arc radius is larger than in the spherical case because the position angle of the arc, in A1689, is roughly perpendicular to that of the second clump; the arc is on the minor axis of the quadrupole moment generated by the secondary clump, and so the critical line has been pushed inward with respect to the spherical case. We have assumed the two clumps to be spherical, and allowance for ellipticity could also change the mass estimate. In the absence of multiple images, no strong constraints are available on the form of the potential. However, the optical image of the cluster and the positions of all the arcs do not suggest a strong ellipticity for the two components, and therefore the correction to the mass within the arc radius from the spherical model is probably small.

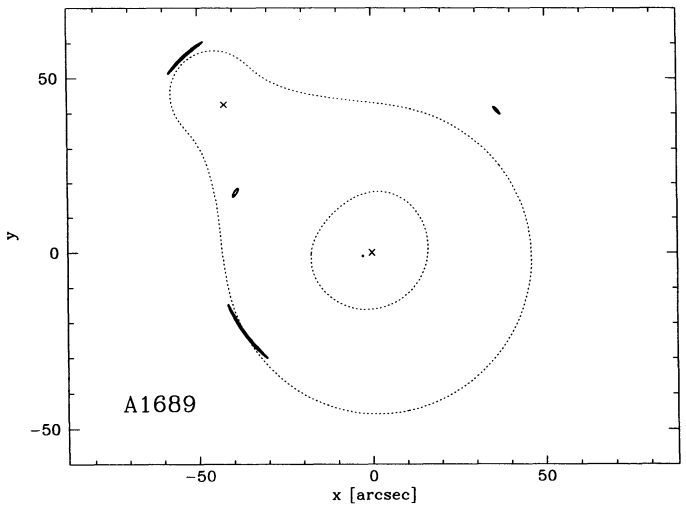

FIG. 3.—Lensing model for A1689, which assumes two mass clumps, corresponding to the large central concentration around galaxy 82 in Gudehus & Hegyi (1991), and the smaller concentration of galaxies 1' to the northeast. The density profiles of the lenses are described by model 1 density profile (eq. [3]); the central lens has parameters $\sigma = 1450$ km s^{-1}, and $r_c/D_l = 10''$, while the secondary lens, at $x = -42''.5$, $y = 42''.5$, has $\sigma = 700$ km s^{-1} and $r_c/D_l = 10''$. Both lenses are assumed to be spherical. One source at $z_s = 3$ produces the long arc close to the secondary clump, and another source at the same redshift yields the fold arc to the southeast of the center, two arclets, and a demagnified image in the center.

3.5. *A1689: Results of X-Ray Fits*

In Figure 4, we show the *Einstein* IPC X-ray surface brightness profile of A1689, as error bars. Alongside, we plot the X-ray profile for isothermal gas of temperature $T_x = 9.5 \times 10^7$ K (*dotted line*) for the best-fitting model 1 mass distribution: $\gamma = 1.5$, $r_c = 1$ Mpc, $F_{cD} = 0.008$. The crosses are the predicted binned fluxes, after convolution with a Gaussian of FWHM = 98″. The χ^2 value for the fit is 116. The solid line depicts the surface brightness for gas whose temperature is twice the observed value, $T_x = 1.9 \times 10^8$ K. The corresponding

predicted binned fluxes are shown as diamonds. In this case, the best-fit model ($\chi^2 = 3.8$) parameters are $r_c = 0.12$ Mpc, $\alpha = 1.0$, $\gamma = 1.56$. If the temperature is increased by a factor of only 1.67 above the observed value, χ^2 increases to 13 (already unacceptable for an expected χ^2 of 5). Similar results are found for model 2. We, therefore, have a similar situation as for A2218: The temperature of the gas needs to be a factor of 2 higher than the observed value, in order to fit the X-ray profile and account for the lensing observations; the observed surface brightness profile is too extended to be compatible with the distribution of gas in pressure equilibrium at the observed temperature in a cluster potential where the amount of projected mass within the radius of the arc is given by equation (2). On the other hand, the best-fit model for $T_x = 1.9 \times 10^8$ K has a very extended mass profile at large radius. If we require the mass profile to fall off more steeply (i.e., $\gamma > 2$), an acceptable fit is obtained only when the gas temperature is 2.2 times the observed value. At this point, it is also worth noting that if the arc is actually at redshift lower than the assumed redshift of $z_s = 3$, the discrepancy between the temperature of the gas in the model and the observed value increases, although the increase is relatively small if $z_s \gtrsim 0.7$.

3.6. *Results for A2163*

The last cluster that we examine is A2163. This cluster differs markedly from A2218 and A1689 in terms of both its X-ray and optical properties. A2163 lies at a redshift of $z_l = 0.2$ and has an X-ray luminosity in the 2–10 keV band of $L_x = 7 \times 10^{45}$ ergs s^{-1}; it is one of the most luminous clusters known. It is also the hottest cluster known, with an X-ray temperature of $kT_x = 13.7 \pm 1$ keV, or 1.6×10^8 K (Arnaud et al. 1992). The *Einstein* IPC image of A2163 is also unusual in the sense that it is not symmetric. Furthermore, its radially averaged X-ray surface brightness profile is very flat at small radii and shallow at large radii. In contrast to its X-ray properties, the optical properties of A2163 are quite unassuming. The cluster galaxies are not very compact and the central galaxy is not a bright cD. A2163 is classified as an Abell richness class 2 cluster. Deep optical images of the cluster reveal two arcs around the central galaxy, at a distance of 15″.6 (J. A. Tyson 1993, private communication). We adopt a value of $b = 15''$ for the critical radius of the cluster. The sources that have been distorted into the arcs lie at $z = 0.728$ and $z = 0.742$ (G. Soucail 1993, private communication); for the purposes at hand, we adopt a source redshift of $z_s = 0.73$. Given the small critical radius and the high X-ray temperature of the gas in the cluster, we expect that there should be no problem in constructing a viable model of the cluster that reproduces the observed surface brightness profile.

In Figure 5, we plot the observed *Einstein* IPC X-ray surface brightness profile of A2163. The model fits are analogous to Figures 2 and 4. The dotted line corresponds to X-ray surface brightness flux emitted by gas at $T_x = 1.4 \times 10^8$ K, with the underlying spherical mass model having the parameters $r_c = 1$ Mpc, $F_{cD} = 0.09$, and $\gamma = 3.80$. The χ^2 value for the fit is 4.5. The solid line corresponds to gas at $T_x = 3.2 \times 10^8$ K and an underlying spherical mass model with parameters $r_c = 0.3$ Mpc, $F_{cD} = 0.01$, and $\gamma = 2.57$. In this case, $\chi^2 = 3.48$. As expected, the model results reproduce the observations well, even if the gas temperature is fixed at its observed value. However, there is a wide range of temperatures over which a good fit can be found, a result that is largely due to the relatively low resolution and signal-to-noise ratio of the IPC X-ray profile.

4. DISCUSSION

In the generally favored bottom-up scenarios where structure in the universe forms hierarchically by gravitational insta-

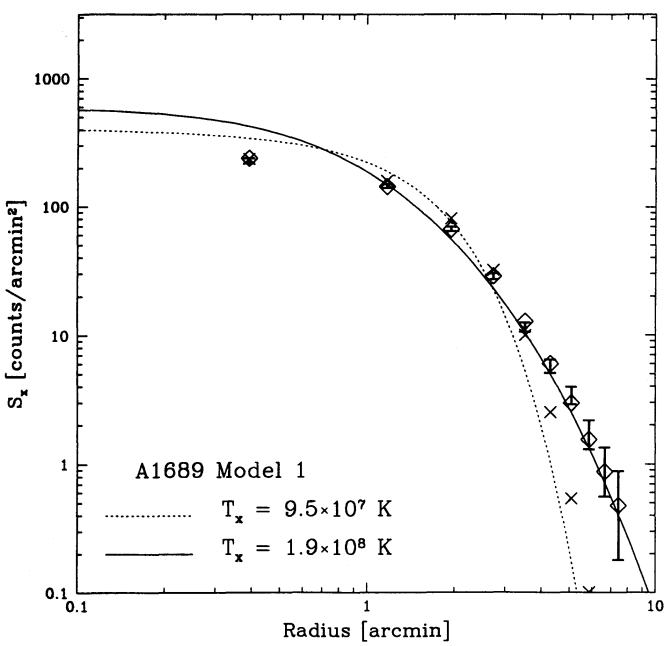

FIG. 4.—Same as Fig. 2*a* but for A1689. When the gas temperature is fixed to the observed value, the best fit has $\chi^2 = 116$. When the temperature is increased by a factor of 2, the fit becomes acceptable with $\chi^2 = 3.8$. Similar results are obtained for model 2.

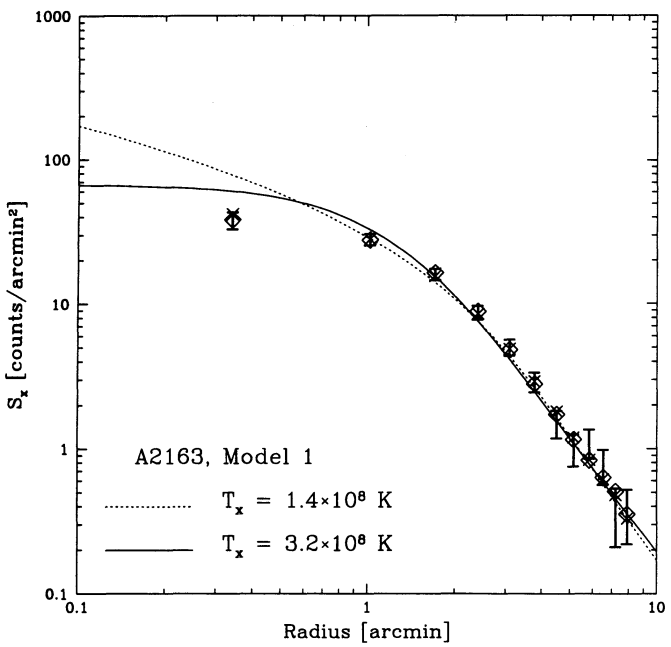

FIG. 5.—Same as Fig. 2*a* but for A2163. In this case, a good fit to the observations is obtained using isothermal gas at a temperature of $T = 1.4 \times 10^8$ K ($\chi^2 = 4.5$), close to the observed temperature, or $T = 3.2 \times 10^8$ K ($\chi^2 = 3.5$).

bility, clusters of galaxies form via merging of smaller mass concentrations. Simulations of clusters, which include both dark as well as baryonic matter, show that as hierarchical clustering proceeds from subcluster to cluster scale, the associated gas suffers repeated shock heating (see Cen & Ostriker 1992; Evrard, Summers, & Davis 1993; Katz & White 1993, and references therein). Each new merger disturbs the state of the gas and it would seem natural to expect that some turbulent and bulk motions must be present. In fact, simulations show that such motions can account for up to 30% of the support of the gas against gravity (Evrard 1990; Navarro, Frenk, & White 1994), although this varies from clusters undergoing mergers to relaxed clusters. It is, however, worth noting that simulation results are very strongly dependent on the range of physical processes incorporated and the resolution of the simulations.

The determination of cluster mass based on X-ray observations rests on the assumption that the gas in real clusters is in hydrostatic equilibrium solely due to thermal pressure. X-ray observations can be used to establish the temperature of the intracluster gas; however, they do not provide any observational tests of the assumption generally adopted in order to derive cluster masses from X-ray observations. With the freedom to choose the underlying total mass density profile, one can fit any combination of observed X-ray temperature and surface brightness profile. The thermal pressure-supported gas hypothesis can be tested only using some independent constraint on the mass distribution. The properties of the galaxy distribution do not provide strong constraints. The uncertainties associated with whether or not galaxies in clusters suffer velocity bias and whether the galaxy orbits are isotropic or not, coupled with the possibility that the optical measurements may be in error as a result of projections effects or be affected by substructure in the clusters, introduce large uncertainties in the cluster mass estimates (Merritt 1987; Babul & Katz 1993). The gravitationally lensed images, on the other hand, offer a direct means of probing the total mass distribution in clusters, and of testing whether the hot intracluster gas is in thermal pressure-supported hydrostatic equilibrium.

Of the three clusters that we have analyzed, the results for one of the clusters, A2163, are ambiguous. On one hand, the cluster X-ray profile is consistent with both the lensing constraints and the gas temperature being pegged at the observed value. On the other hand, the observed X-ray profile is also consistent with a model where the gas temperature is twice as large as that observed. It should, however, be borne in mind that A2163 is a rather unusual cluster. Its X-ray image is very extended and shows signs of substructure. It is possible that the cluster is in the process of relaxing, where the gas has been shock-heated up to the cluster virial temperature but the dark matter has not yet relaxed into a smooth, centrally concentrated distribution. The galaxy distribution is also consistent with a weakly concentrated cluster. In this case, the two arcs around the brightest galaxy may reflect only the potential well of one of several subclumps merging to form the cluster. This may explain why the hottest and most X-ray luminous cluster known shows only two small arcs with a relatively small critical radius.

In the case of A2218 and A1689, we find that it is not possible for the gas to be supported against gravity solely by thermal pressure in a spherical model. For the gas to be thus supported, it must either have a temperature that is a factor of 2–3 times greater than the observed value, if the gas is isothermal, or there must exist a temperature gradient that ought to have been detected. We consider below various other explanations for resolving the discrepancy:

1. The large mass estimate obtained from lensing might be a consequence of our having adopted an $\Omega = 1$ cosmological model for the universe. However, the inferred mass with a given observed critical radius depends only on the distance ratio D_{ls}/D_s, which is very insensitive to cosmology (e.g., Blandford & Kochanek 1988). We also note that both the lensing and X-ray masses scale as H_0^{-1}.

2. The mass estimates based on the lensing argument may be overestimated because the projected cluster potentials may differ significantly from circular symmetry. However, as we have seen, in the case of A2218, the mass within the critical radius implied by lensing is reduced only by a factor 1.15 in a model which incorporates the ellipticity of the main mass clump and also the effect of the secondary mass clump. In the case of A1689, the projected mass is actually higher by a factor 1.04 in an aspherical model that reflects the double-clump structure suggested by the distribution of cluster galaxies and the observed arcs. In the latter case (A1689), it is also likely that the arc lies at a lower redshift than assumed, once again implying that our mass estimate is a lower limit.

3. The clusters A2218 and A1689 may be highly prolate, with the long axis aligned along the line of sight. From among a sample of clusters of some fixed total mass, those that are highly prolate and well-aligned along the line of sight have a higher probability of producing arcs. They should also appear richer and more compact in optical as a result of the increased galaxian surface density, increasing the likelihood of their discovery and inclusion in optical catalogs (Miralda-Escudé 1993). To see the magnitude of the effect, consider a spherical cluster and stretch it along the line of sight by a factor $q > 1$ while compressing it along the other two perpendicular axes by a factor $q^{-1/2}$ (so the total mass as a function of radius remains unchanged). The stretching causes an increase of the surface density by a factor q, and the transverse compression results in an increase in the surface mass density, which depends on how fast the surface density is decreasing with radius. Thus, the actual amount by which the surface mass density is enhanced depends on the mass density profile in the cluster, but it is always less than q (the enhancement factor is close to q when the surface density is nearly constant within the critical radius, and it becomes smaller as the surface density profile steepens). At the same time, the gas distribution will also be elongated (although less than the mass, since the gas density is constant on equipotential surfaces), and the X-ray profile will appear more concentrated than in a spherical cluster, therefore increasing also the mass within the critical radius derived from the X-ray profile. Thus, a factor of 2 enhancement of the surface density, relative to the value derived from X-ray observations, requires an axis ratio of the mass distribution larger than ~ 3–4, with the major axis very well aligned along the line of sight. This is a rather rare combination of configuration and orientation, and it is unlikely that prolateness and alignment is the sole explanation for the discrepancy, although it could be a contributing factor.

Alternatively, the projection effect may be due to superposition of two mass clumps along the line of sight. If the two clumps are of nearly equal mass, and the gas in each subcluster is in hydrostatic equilibrium, undisturbed by the other clump, the temperature of the gas would reflect only the mass of a

single subcluster, while both mass clumps would contribute toward gravitational lensing. Although a double-clump structure is observed in both A2218 and A1689, it is unlikely that the two clumps are acting in unison in order to produce the lensing. The angular separation of the subclusters in each of the clusters places them outside each other's critical radius and also, the central mass concentration in A2218 and A1689 appears to be much more massive than the secondary concentration, as deduced both from the light observed in each clump and from the modeling of the various observed arcs. Therefore, the observed subclusters do not appear to be sufficiently well aligned to explain the discrepancy. On the other hand, it is possible that an unobserved mass clump may be involved; after all, there is mounting evidence suggesting that the present-day clusters are conglomerates of subclusters that are presumably in the process of merging. For example, the *ROSAT* HRI image of cluster A370 has revealed two previously unresolved peaks that are coincident with the two central galaxies (H. Bohringer & Y. Mellier 1993, private communication), confirming the expectations regarding the nature of the cluster potential based on the fact that the two central galaxies are both equally luminous, equally extended, and that the lensing models of A370 require a double-peaked surface mass distribution (Kneib et al. 1993). Also, many of the clusters in the ESO cluster redshift survey (see Mazure et al. 1991) show features that imply a great deal of substructure (P. Katgert 1993, private communications).

4. Substructure in the clusters may also help solve the mystery of the discrepant mass estimates if mass clumps manage to impart bulk motions to the gas in the central regions as they fall through. Hydrodynamical simulations of clusters suggest that during quiescent periods, the gas is primarily supported by thermal pressure; however, the bulk motions might account for 20%–30% of the support during mergers (Evrard 1990; Navarro et al. 1994). The response of the gas to subclumps ploughing through the main cluster body has simply not been well studied. Bulk or turbulent motions would allow the gas residing in a potential with a small core radius to have an extended core without being hotter than observed. The main problem with this explanation is that such motions should quickly dissipate after the merger is over. Coherent motions such as rotation arising during the collapse of the dark halos are very small (Barnes & Efstathiou 1987) and therefore, if the gas is to be rotationally supported, the gas must have experienced a large amount of dissipation. This seems inconsistent with the small ratios of gas mass to total mass observed in cluster centers (e.g., Edge & Stewart 1991).

5. The gas may be supported in part by magnetic pressure. Determinations of the general cluster fields using Faraday rotation measures of background or cluster radio sources suggest that overall the intracluster magnetic field is too weak to have any important dynamical influence (Sarazin 1992). In the central regions, however, magnetic fields could be enormously amplified by compression and inflow associated with cooling flows. If magnetic fields are present, they would have to vary on very small scales in order to agree with the observed excess of Faraday rotation in radio sources behind clusters (Kim, Tribble, & Kronberg 1991). At the same time, if the field is dynamically important, the magnetic lines cannot be bent with a radius of curvature much smaller than the pressure scale height, otherwise the lines would straighten out because there cannot be any force balancing the magnetic force. The only possibility seems to be to have long tubes of magnetic field with alternating polarity on very small scales, but it is not clear how such a configuration might be created.

6. The intracluster medium in the central regions of the cluster should be inhomogeneous, due to the rapid cooling rate of the gas (e.g., Thomas, Fabian, & Nulsen 1987). A multiphase medium has the advantage of allowing for a high effective temperature (i.e., pressure divided by average gas density) that could account for the extended gas core, while not being in conflict with the lower temperatures derived from the emission-weighted X-ray spectra (e.g., Schwarz et al. 1992). A multiphase medium with high temperatures, however, is constrained by the upper limits on the excess of high-energy photons in X-ray spectra, with respect to the emission from a single-temperature gas (Allen et al. 1992).

5. SUMMARY AND CONCLUSIONS

In this paper, we examined three clusters in which long arcs have been observed and whose X-ray properties have been well studied. We find that the mass estimate derived from gravitational lensing considerations can be as much as a factor of 2–2.5 larger than the mass estimate derived from analysis of the X-ray observations. We have considered various possible explanations for the discrepancy. Of these, those that are most promising fall into one of the following categories.

1. Projection effects, where either the clusters themselves are highly prolate and well-aligned along the line of sight, or the cluster consists of at least two main clumps that are aligned sufficiently well so as to be hidden by projection in the X-ray maps.
2. A temperature profile that rises toward the center.
3. Inhomogeneous intracluster medium, where the gas, particularly in the central region, is a multiphase medium.
4. Nonthermal pressure support, where the gas, particularly in the central region, is supported in part by bulk motions and/or by magnetic fields.

As discussed before, none of these four explanations seems particularly likely to account for the entire problem; it seems more plausible to us that a combination of all of them will turn out to be the solution. In this sense, it is reassuring that all of the effects that can cause a systematic discrepancy between the masses derived from X-ray and lensing observations go in the right direction to explain the observed difference.

In order to unravel further the mystery underlying the discrepancy, the sample of clusters for which both lensing and X-ray observations (temperature and surface brightness profile) are available, needs to be enlarged and thoroughly analyzed. The following observations would be most relevant.

1. High-resolution X-ray images of the central regions of the clusters—in order to test for the presence of substructure in the X-ray emissivity.
2. Acquisition of more arc redshifts—in order to allow for improvements to existing lensing models.
3. Measurements of X-ray temperatures in more clusters with lensing observations—in order to increase the sample where the comparison of masses we have presented here can be made, and to improve mass estimates derived from X-ray observations. This may prove difficult for the faint high-redshift clusters, but the X-ray luminosity-temperature relationship may be used.
4. Measurements of the high-energy spectrum of a large number of clusters—in order to test for the presence of a hot

phase in the intracluster gas and thereby constrain the multiphase medium hypothesis.

5. Observations of the weakly distorted background galaxies—in order to reconstruct the surface density of the clusters (see Tyson et al. 1990; Kaiser & Squires 1993), and improve the cluster mass distribution models based only on constraints provided by the long arcs. This would be particularly useful in an X-ray selected sample, to avoid biases due to projection effects. Since weak lensing analysis provides a mass estimate with an approximately constant relative accuracy with radius (Miralda-Escudé 1991), it should be possible to check whether the discrepancy between the lensing and the X-ray mass estimates extends to large radii. If so, it is possible that part of the explanation for why the apparent fraction of baryonic mass in clusters, as derived from the X-ray data, is much larger than the cosmological baryon fraction implied by the standard theory of cosmic nucleosynthetis in an $\Omega = 1$ universe (see Babul & Katz 1993; White et al. 1993 and references therein) may be due to the fact that the X-ray mass estimates are actually underestimates.

On the theoretical side, the hydrodynamical simulations of clusters need to be improved to the point where the treatment of the gas in the central regions of the clusters is realistic and reasonably well resolved. Such simulations are needed to determine the influence of substructure and the importance of bulk motions. The effects of cooling flows on the temperature profile and temperature distribution in an inhomogeneous medium (Thomas 1988 and references therein), taking into account the deep potential wells implied by gravitational lensing, should also be better studied. If the X-ray surface brightness profile of the gas in the simulated clusters have smaller cores than observed, this may indicate that not all of the important physical processes in the intracluster medium have been taken into consideration.

We would like to thank Tony Tyson for allowing us access to unpublished lensing data for A2163, and Genevieve Soucail for informing us on the redshift measurements. We are also indebted to Alastair Edge and Gordon Stewart for providing us with the *ROSAT* image of A2218 in advance of publication. In addition, Alastair Edge helped us obtain the *Einstein* data for A1689 and A2163, and was a source of useful comments. Finally, we would like to acknowledge many stimulating discussion with Hans Böhringer, Carlos Frenk, "Raja" Guhathakurta, Yannick Mellier, Martin Rees, Peter Tribble, Simon White, and Eli Waxman. A. B. acknowledges the hospitality of the Institute of Astronomy (University of Cambridge) over the course of his visits during the summers of 1992 and 1993. J. M. thanks SERC for support in the Institute of Astronomy, and the W. M. Keck Foundation for support in the Institute for Advanced Study.

REFERENCES

Allen, S. W., Fabian, A. C., Johnstone, R. M., Nulsen, P. E. J., & Edge, A. C. 1992, MNRAS, 254, 51
Arnaud, M., Hughes, J. P., Forman, W., Jones, C., Lachieze-Rey, M., Yamashita, K., & Hatsukade, I. 1992, ApJ, 390, 345
Babul, A., & Katz, N. 1993, ApJ, 406, L51
Barnes, J., & Efstathiou, G. 1987, ApJ, 319, 575
Blandford, R. D., & Kochanek, C. S. 1987, in 4th Jerusalem Winter School on Dark Matter in the Universe, ed. J. Bahcall, T. Piran, & S. Weinberg (Singapore: World Scientific), 133
Cen, R. Y., & Ostriker, J. P. 1992, ApJ, 393, 22
David, L. P., Slyz, A., Jones, C., Forman, W., Vrtilek, S. D., & Arnaud, K. A. 1993, ApJ, 412, 479
Edge, A. C., & Stewart, G. C. 1991, MNRAS, 252, 414
Einstein, A. 1936, Science, 84, 506
Evrard, A. E. 1990, ApJ, 363, 349
Evrard, A. E., Summers, F. J., & Davis, M. 1993, ApJ, 422, 11
Grossman, S. A., & Narayan, R. 1988, ApJ, 324, L37
———. 1989, ApJ, 344, 637
Gudehus, D. H. 1989, ApJ, 340, 661
Gudehus, D. H., & Hegyi, D. J. 1991, AJ, 101, 18
Hammer, F. 1991, ApJ, 383, 66
Jones, C., & Forman, W. 1984, ApJ, 276, 38
Kaiser, N., & Squires, G. 1993, ApJ, 404, 441
Katz, N., & White, S. D. M. 1993, ApJ, 412, 455
Kellogg, E., Falco, E., Forman, W., Jones, C., & Slane, P. 1990, in Gravitational Lensing, ed. Y. Mellier, B. Fort, & G. Soucail (Berlin: Springer), 141
Kim, K. T., Tribble, P. C., & Kronberg, P. P. 1991, ApJ, 379, 80
Kneib, J. P., Mellier, Y., Fort, B., & Mathez, G. 1993, A&A, 273, 367
Kneib, J. P., Mellier, Y., Pelló, R., Miralda-Escudé, J., Le Borgne, J. F., Böhringer, H., & Picat, J. P. 1994, A&A, submitted
Le Borgne, J. F., Pelló, R., & Sanahuja, B. 1992, A&AS, 95, 87
Lynds, R., & Petrosian, V. 1989, ApJ, 336, 1
Mazure, A., et al. 1991, ESO Messenger, 65, 7
McHardy, I. M., Stewart, G. C., Edge, A. C., Cooke, B., Yamashita, K., & Hatsukade, I. 1990, MNRAS, 242, 215
Mellier, Y., Fort, B., & Kneib, J.-P. 1993, ApJ, 407, 33
Merritt, D. 1987, ApJ, 313, 121
Miralda-Escudé, J. 1991, ApJ, 370, 1
———. 1993, ApJ, 403, 497
Miralda-Escudé, J., & Babul, A. 1994, in Cosmological Applications of X-Ray Clusters of Galaxies, ed. W. Seitter et al. (Dordrecht: Kluwer), in press
Narayan, R., Blandford, R., & Nityananda, R. 1984, Nature, 310, 112
Navarro, J. F., Frenk, C. S., & White, S. D. M. 1994, MNRAS, in press
Pelló, R., Le Borgne, J. F., Sanahuja, B., Mathez, G., & Fort, B. 1992, A&A, 266, 6
Pelló, R., Soucail, G., Sanahuja, B., Mathez, G., & Ojero, E. 1988, A&A, 190, L11
Petrosian, V., & Lynds, R. 1992, in Gravitational Lenses, ed. R. Kayser, T. Schramm, & L. Nieser (Berlin: Springer), 305
Sarazin, C. L. 1992, in Clusters and Superclusters of Galaxies, ed. A. C. Fabian (Dordrecht: Kluwer), 131
Schwarz, R. A., Edge, A. C., Voges, W., Bohringer, H., Ebeling, H., & Briel, U. G. 1992, A&A, 256, L11
Soucail, G., Fort, B., Mellier, Y., & Picat, J.P. 1987, 172, L14
Stewart, G. C., et al. 1994, in preparation
Thomas, P. A. 1988, MNRAS, 235, 315
Thomas, P. A., Fabian, A. C., & Nulsen, P. E. J. 1987, MNRAS, 228, 973
Turner, E. L., Ostriker, J. P., & Gott, J. R. 1984, ApJ, 284, 1
Tyson, J. A., Valdes, F., & Wenk, R. 1990, ApJ, 349, L1
Walsh, D., Carswell, R. F., & Weymann, R. J. 1979, Nature, 279, 381
White, S. D. M., Navarro, J., Evrard, A., & Frenk, C. S. 1993, Nature, 366, 429
Wu, X., & Hammer, F. 1993, MNRAS, 262, 187
Yamashita, K. 1994a, to appear in the Proceedings of the Rencontres de Moriond Conference Clusters of Galaxies, ed. F. Durret et al.
———. 1994b, private communication
Zwicky, F. 1937, Phys. Rev. Lett., 51. 290